

Analysis of Age-Energy Trade-off in IoT Networks Using Stochastic Geometry

Songita Das, *Graduate Student Member, IEEE* and Gourab Ghatak, *Member, IEEE*

Abstract—We study an internet of things (IoT) network where devices harvest energy from transmitter power. IoT devices use this harvested energy to operate and decode data packets. We propose a slot division scheme based on a parameter ξ , where the first phase is for energy harvesting (EH) and the second phase is for data transmission. We define the joint success probability (JSP) metric as the probability of the event that both the harvested energy and the received signal-to-interference ratio (SIR) exceed their respective thresholds. We provide lower and upper bounds of (JSP), as obtaining an exact JSP expression is challenging. Then, the peak age-of-information (PAoI) of data packets is determined using this framework. Higher slot intervals for EH reduce data transmission time, requiring higher link rates. In contrast, a lower EH slot interval will leave IoT devices without enough energy to decode the packets. We demonstrate that both non-preemptive and preemptive queuing disciplines may have the same optimal slot partitioning factor for maximizing the JSP and minimizing the PAoI. For different transmit powers and deployment areas, we recommend the optimal slot partitioning factor for the above two metrics under both queuing disciplines.

Index Terms—Radio-Frequency (RF), Joint Success Probability (JSP), Peak Age of Information (PAoI), Energy Harvested (EH), Stochastic Geometry, Internet of Things (IoT), Preemptive (P), Non-Preemptive (NP), Linear (L), Non-Linear (NL).

I. INTRODUCTION

A. Context and Motivation

THE age of information (AoI) is a metric used in communication networks to assess how quickly information reaches its destination in relation to when it was created at the source [2]. Contrary to the classical wireless performance metrics such as throughput and delay that characterize data transfer efficiency, the AoI adequately takes into account the freshness of data. This makes it attractive for system design in real-time internet of things (IoT) applications [3]. Traditional performance metrics include latency and reliability, where latency refers to the time taken for data to travel from the source to the destination, while reliability measures the likelihood of delivering data without errors or loss. However, even in systems with low latency and high reliability, the AoI can be high, indicating that the data, though transmitted quickly and accurately, may be outdated by the time it is received. For example, in autonomous vehicle communication [4] and drone

swarm coordination [5], vehicles and drones communicate data regarding speed and position to ensure safety. Nonetheless, if updates occur infrequently and conditions fluctuate rapidly, even low-latency and reliable data may become obsolete, leading to a high AoI. For instance, if a drone alters its position or a car abruptly brakes after transmitting an update, subsequent drones or vehicles may receive obsolete information, jeopardizing safety and heightening the risk of collisions or mission failure, despite the system's low latency and high reliability. It is to be noted that in systems featuring multiple devices transmitting simultaneously, interference deteriorates communication, resulting in missed or erroneous updates that may cause collisions or other significant problems. Conversely, noise generally diminishes signal quality without entirely obstructing communication. Commonly employed downlink techniques in drone swarm coordination are dedicated ground control systems, which act as the central hub for delivering commands and data to drones. In situations where drones communicate via cellular networks, a central control system or cloud server transmits real-time updates and commands via the cellular network. Likewise, in satellite communication, the central control system uses a satellite link to send commands or data to drones thereby facilitating long-range communication.

Additionally, the devices for such IoT applications are often battery-constrained, and regular battery replacements are infeasible. To alleviate this energy harvesting (EH) is a key solution that converts ambient energy into usable electrical power [6]. EH provides a supplemental or alternative power source, allowing devices to run independently and sustainably [7]. Since the wireless signals are repurposed for EH, often it has an adverse impact on the decoding of the received signals, and consequently, the AoI. Hence, the joint characterization and optimization of EH and AoI in wireless networks is critical and is the focus of this paper.

B. Literature Review

Abd-Elmagid *et al.* [8] provide a comprehensive overview of AoI and its variants and their utility in designing freshness-aware IoT networks. They contrast the key differences of AoI with respect to classical wireless network performance metrics such as throughput and delay. Furthermore, they reveal achievable AoI regions with optimal energy sampling and transmission policies. Yates and Kaul [9] analyzed AoI in queues for stochastic hybrid systems that utilize memory-less service. Indeed, AoI and its optimization have been the subject of extensive research in a variety of network scenarios in order to improve the freshness of data. Chen *et al.* [10] studied multi-

The preliminary version of this paper was presented at the 22nd International Symposium on Modeling and Optimization in Mobile, Ad hoc, and Wireless Networks. WiOpt, RAWNET workshop, 2024 [1]. Songita Das is with the Bharti School of Telecommunication Technology and Management, Indian Institute of Technology Delhi, New Delhi 110016, India (email: bsz228102@iitd.ac.in). Gourab Ghatak is with the Department of Electrical Engineering, Indian Institute of Technology Delhi, New Delhi 110016, India (email: gghatak@ee.iitd.ac.in).

hop wireless sensor nodes (WSNs) that employ EH while optimizing AoI. In particular, they formulate a problem that is NP-hard in order to minimize the same. Consequently, they propose an algorithm MA_{AoI} and characterize the bounds on peak age of information (PAoI) and average AoI achieved by their algorithm. On the contrary, Zhu *et al.* [11] focused on the scheduling challenges associated with minimizing AoI in battery-free one-hop WSNs by employing a variety of EH strategies. In particular, the authors discuss the optimal offline policy and introduce competitive online policies for minimizing AoI. Zhang *et al.* [12] investigated the impact of deploying mobile edge computing (MEC) servers on the computational ability of the sensor nodes. They formulated a non-convex problem to optimize the sampling rate, computation rate, and the AoI, and proposed a successive convex approximation technique to solve the same. Kim *et al.* [13] investigated optimal duty cycles for self-sustaining operations. For further works on joint AoI and EH optimization, we refer the reader to the references [14]–[21].

Rigorous optimization procedures, although useful for specific network instances, do not provide insights into the variance of performance measures across different network realizations. In this regard, stochastic geometry provides useful tools for the statistical characterization of such networks, thereby enabling the derivation of key system-design insights and dimensioning rules. Leveraging stochastic geometry, Mankar *et al.* [22] study both preemptive and non-preemptive queuing and their impact on the AoI in large-scale wireless networks constituting source-destination pairs. In particular, they derive tight bounds on the moments and spatial distribution of PAoI using a bipolar Poisson point process model, which are validated through numerical results. Abd-Elmagid *et al.* [23] investigate the joint transmission coverage and energy harvesting performance in a network with node locations modeled as a Poisson cluster process (PCP). They state that computing the distribution of shot noise processes associated with the PCP is challenging. Consequently, they prescribe approximations for the characterization of joint signal and energy coverage. Yang *et al.* [24] have analyzed the spatio-temporal performance of AoI by using queuing theory in conjunction with stochastic geometry. They showed that a decentralized scheduling policy reduces AoI through local observations. The suggested method adjusts radio access probabilities to accommodate traffic changes to reduce PAoI, and accommodate network expansion. Furthermore, they extended their investigation in [25] to show that the last-come, first-served (LCFS) order has a variable impact on AoI in relation to the deployment density, while the slotted ALOHA protocol does not reduce AoI at low packet arrival rates.

Very few studies [26], [27] have investigated EH and AoI jointly in uplink stochastic geometry frameworks, where source nodes perform EH. In [26], the authors have characterized the AoI performance of the users by considering their EH capabilities. Based on their formulation, they have optimized the channel access policy that minimizes the AoI. On the contrary, [27] has studied the distributional properties of AoI by assuming that the status packets and the energy packets arrive at the devices following a Poisson arrival process. This

enhances our understanding of the statistics of the AoI along with EH capabilities. However, none of the existing works derive the efficacy of the EH process jointly with the AoI. In particular, when fewer transmit nodes are located in the network, this not only enhances the signal coverage due to limited interference but also reduces the ability of the users to effectively harvest energy. In order to jointly study this, we introduce the term called joint success probability (JSP) and investigate how the temporal resources can be partitioned in order to maximize either the JSP or minimize the PAoI.

C. Contributions

We consider an energy-harvesting IoT network where the IoT devices operate with harvested energy from the transmitters of the network. Given that the devices have harvested sufficient energy, they attempt to decode the downlink transmissions from the base stations (BS). Based on this system, we make the following contributions:

- 1) First, we study non linear energy harvesting (NL EH) based on which we derive the probability of the joint event that the harvested energy at the device exceeds an energy threshold and that the downlink signal to interference ratio (SIR) exceeds an SIR threshold. We term this as the JSP and it determines the ability of any device in the network to simultaneously harvest the necessary energy to operate and the ability to decode the downlink data. To the best of our knowledge, this joint characterization has not yet been studied in stochastic geometry frameworks.
- 2) In order to allot resources between the EH and the data transmission functionalities, we consider a slotted frame design. Next, based on the derived JSP and by considering the slotted frame, we characterize the PAoI at the IoT devices with respect to the frame partitioning factor ξ .
- 3) Interestingly, we show that for every given value of transmit power, there exists a unique optimal slot partitioning factor ξ^* that, in both the preemptive and non-preemptive queuing disciplines, maximizes JSP while minimizing PAoI for a disc of a specific radius. Following this, we derive several system design insights. Based on the application of interest, the value of ξ must be tuned appropriately.

II. SYSTEM MODEL AND PROBLEM FORMULATION

A. Network Geometry

We consider an IoT network wherein the IoT devices are served by their nearest transmitter. Let the locations of the IoT devices be denoted by s_n , $n \in \{1, \dots, N\}$. The transmitter locations are denoted by r_k . The typical IoT device is denoted by s_1 while the location of the transmitter closest to the typical IoT device is denoted by r_1 . The transmitter locations are modeled as a Poisson point process (PPP), Φ with intensity λ in a disk $\mathcal{B}(s_1, R)$ of radius R centered at s_1 . The distances between the typical IoT device and the typical transmitter are represented by $d_1 = \|s_1 - r_1\|$ and the distances from the typical IoT device to any other transmitter are represented by $d_k = \|s_1 - r_k\|$.

B. Propagation Model

Let the transmit power multiplied by the path-loss constant for all the transmitters be P_t . Accordingly, the power received by the typical IoT device from the associated transmitter in the j -th slot is given by $P_{R_1} = P_t g_1^j d_1^{-\alpha}$ while the interference power is given by $P_{R_k} = P_t \sum_{k=2}^K g_k^j d_k^{-\alpha}$. The small-scale fading gains are assumed to be exponentially distributed and denoted by g_1^j for the typical transmitter and g_k^j for the k -th interfering transmitter. Due to the PPP assumption for the location of the interferers, K is a Poisson distributed random variable with parameter $\lambda\pi R^2$. Assume that each time slot is of duration τ , and is divided into two distinct phases—an EH phase of duration $\xi\tau$ and a data transmission phase of duration $(1-\xi)\tau$. During the EH phase, the IoT device harvests RF energy from the downlink transmissions of all the transmitters. While, during the data transmission phase, the typical IoT device uses the harvested energy to decode the packet received from the typical transmitter. Let E_1^j represent the energy harvested by the typical IoT device in the j^{th} time slot. It has two components: the desired signal and the interfering signals. Mathematically,

$$E_1^j = \xi\tau P_{R_1} = \eta\xi\tau P_t \left(g_1^j d_1^{-\alpha} + \sum_{k=2}^K g_k^j d_k^{-\alpha} \right). \quad (1)$$

where, η represents energy efficiency. The typical IoT device must harvest more than E_{th} amount of energy to be able to power its receiving circuitry and, hence, receive data successfully during the information reception phase. In order to initiate the harvesting process, the input of any practical harvesting circuit must exceed the minimum power (Pr_{min}). Furthermore, the output of these harvesting circuits becomes saturated when the input power reaches the saturation threshold (Pr_{max}), resulting in a constant output despite fluctuations in input power. Therefore, the energy that is harvested in the non-linear scenario can be assessed as

$$E_1^j = \begin{cases} 0 & , Pr < Pr_{min} \\ \eta\xi\tau P_t (g_1 d_1^{-\alpha} + \sum_{k=2}^K g_k d_k^{-\alpha}) & , Pr_{min} < Pr < Pr_{max} \\ \eta\xi\tau Pr_{max} & , Pr_{max} < Pr \end{cases} \quad (2)$$

where, $Pr_{min} = P_t (g_1 d_1^{-\alpha} + d_K^{-\alpha} \sum_{k=2}^K g_k)$, $Pr = P_t (g_1 d_1^{-\alpha} + \sum_{k=2}^K g_k d_k^{-\alpha})$ and $Pr_{max} = P_t (g_1 d_1^{-\alpha} + d_1^{-\alpha} \sum_{k=2}^K g_k)$

Let Υ_1^j represent the SIR measured at the typical IoT device and it is the ratio of the signal power to the interference power received at s_1 in the j^{th} time slot. Mathematically,

$$\Upsilon_1^j = \frac{P_t g_1^j d_1^{-\alpha}}{\sum_{k=2}^K P_t g_k^j d_k^{-\alpha}}. \quad (3)$$

In order to successfully decode the data packet, the SIR at the typical IoT device must be greater than an SIR threshold β . Let the number of bits to be transmitted be given by σ during the $(1-\xi)\tau$ fraction of the slot dedicated for data transmission. Furthermore, let the required data rate, r is given by $r = \frac{\sigma}{(1-\xi)\tau}$. From the Shannon-Hartley theorem, the maximum data rate is the channel capacity, i.e., $C = B \log_2(1 + \Upsilon_1^j)$,

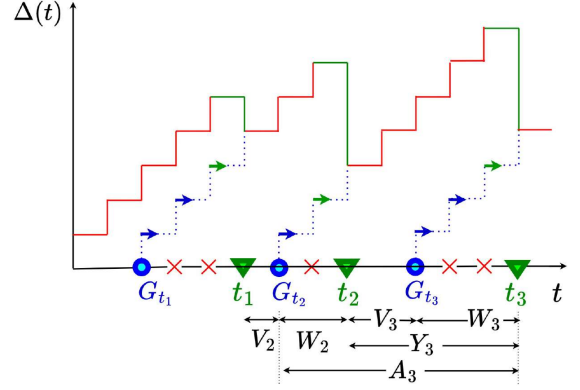


Fig. 1. Illustration of sample path of AoI under non-preemptive queue discipline.

where B is the bandwidth of the channel. Thus, for transmission success, we need $C > r$ or $\Upsilon_1^j > 2^{\frac{r}{B}} - 1$. Thus, we set our SIR threshold as $\beta = 2^{\frac{r}{B}} - 1$.

C. Performance Metrics of Interest

Our main metrics of interest are JSP and PAoI denoted by μ_ϕ and A_i , respectively.

Definition 1. The JSP, μ_ϕ is defined as the probability of the joint event that the harvested energy exceeds the energy threshold E_{th} and the downlink SIR exceeds the SIR threshold β . Mathematically,

$$\mu_\phi = \mathbb{P}[E_1^j > E_{th}, \Upsilon_1^j > \beta]. \quad (4)$$

Definition 2. The AoI, $\Delta(t)$ at time slot t is defined as the time elapsed since the last received packet at the IoT device was generated at the transmitter. Let G_{t_i} and t_i denote the generation and reception time instants of the i^{th} packet at the transmitter and the IoT device, respectively. Mathematically,

$$\Delta(t+1) = \begin{cases} \Delta(t) + 1, & \text{if transmission fails,} \\ t_i - G_{t_i} + 1, & \text{otherwise.} \end{cases} \quad (5)$$

Thus, $\Delta(t)$ increases in a staircase fashion with time slots and drops upon reception of a new packet at the destination, to the total number of slots experienced by this new packet in the system. The typical IoT device experiences interference from other transmitters.

D. AoI under Non-Preemptive Queue Discipline

We assume a non-preemptive queuing model. Let the packets arrive at the transmitter following a Bernoulli process with probability p_a at each time slot. On the arrival of a new packet, the transmitter attempts to send this packet to the IoT device at each consecutive time slot. Until the transmission is successful, newly arrived packets are dropped. Let $W_i = t_i - G_{t_i}$ denote the time slots required for successful transmission of the i -th arrived packet. On successful delivery of the packet at the IoT device, the transmitter admits new packets. Let V_i denote the time slots between the successful delivery of the $(i-1)$ -th packet and the arrival of the i -th packet. Thus,

$$Y_i = W_i + V_i, \quad (6)$$

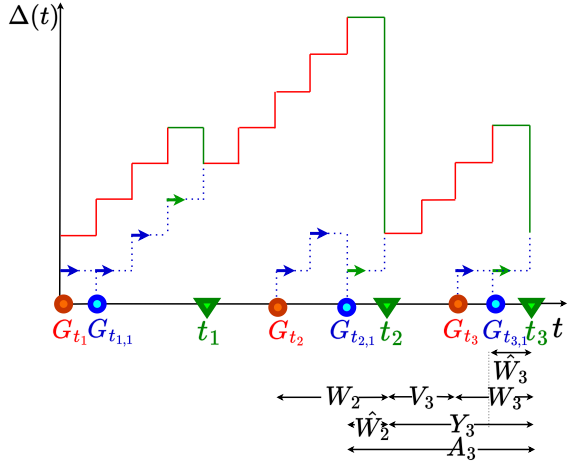


Fig. 2. Illustration of sample path of AoI under preemptive queue discipline.

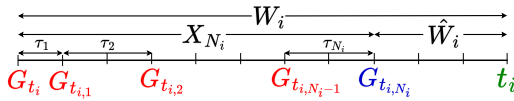


Fig. 3. Illustration of the process \hat{W}_i under preemptive queue discipline.

denotes the time elapsed between the successful delivery of the $(i-1)$ -th and the i -th packets. In a given time slot, both the EH and SIR at the typical IoT must surpass the E_{th} and β thresholds simultaneously for packet transmission to be successful, the probability of which is determined by μ_ϕ . Thus, given the arrival of a packet for transmission, the success event at each time slot is independent and identically distributed. Accordingly, the transmissions on a typical link can be represented using a Geo/Geo/1 model.

Fig. 1 depicts an AoI process sample path. Crosses indicate instances of packets being dropped during server activity of i^{th} packet trying to reach the destination. Then, the PAoI, A_i , corresponding to the i -th packet measures the maximum time elapsed since the last received, i.e., the $(i-1)$ -th packet at the destination was generated. This is given by

$$A_i = W_{i-1} + Y_i. \quad (7)$$

E. AoI under Preemptive Queue Discipline

In preemptive discipline, each source transmits its most recent update in a given slot, reducing the AoI, especially when updates arrive frequently but delivery is slow. This approach is optimal for minimizing AoI, as the latest update is always transmitted. Fig. 2 illustrates the AoI process, where G_{t_i} show update arrivals, t_i show deliveries, and $G_{t_{i,n}}$ indicate when older updates are replaced by newer ones. This term marks the n -th replacement of the i -th update.

Let the packets arrive at the transmitter following a Bernoulli process with probability p_a at each time slot. On the arrival of a new packet, the transmitter attempts to send this packet to the IoT device at each consecutive time slot. If a new packet arrives at the transmitter, then the packet in service is dropped and the newly arrived packet starts getting serviced at each consecutive time slot. Let $W_i = t_i - G_{t_i}$ denote the time slots required for the successful reception of the i -th

packet at the destination. \hat{W}_i denotes the number of time slots required to deliver the latest n -th replacement of the i -th packet at the destination and is given by $\hat{W}_i = W_i - X_{N_i}$, where, $X_{N_i} = \sum_{n=1}^{N_i} \tau_n$ and N_i is the number of new replacement packet arrivals occurring between the arrival and successful delivery of the i -th packet at the transmitter and destination IoT device, respectively. Fig. 3 illustrates the process \hat{W}_i under preemptive queue discipline. τ_n is the number of slots between the arrivals of two successive packet replacements that are i.i.d. and follow a geometric distribution with parameter p_a .

On successful delivery of the packet at the IoT device, the transmitter admits new packets. Let V_i denote the time slots between the successful delivery of the $(i-1)$ -th packet and the arrival of the i -th packet. Thus,

$$Y_i = W_i + V_i, \quad (8)$$

denotes the time elapsed between the successful delivery of the $(i-1)$ -th and the i -th packets. In a given time slot, both the EH and SIR at the typical IoT must surpass the E_{th} and β thresholds simultaneously for packet transmission to be successful, the probability of which is determined by μ_ϕ . Thus, given the arrival of a packet for transmission, the success event at each time slot is independent and identically distributed. Accordingly, the transmissions on a typical link can be represented using a Geo/Geo/1 model.

Fig. 2 depicts an AoI process sample path where we observe that the PAoI, A_i , corresponding to the i -th packet measures the maximum time elapsed since the last received packet (i.e. the $(i-1)$ -th packet received at t_{i-1}) at the destination, was generated (i.e. the n -th replacement of the $(i-1)$ -th packet was generated at $G_{t_{i-1,n}}$) at the source. This is given by

$$A_i = \hat{W}_{i-1} + Y_i. \quad (9)$$

III. JOINT SUCCESS PROBABILITY ANALYSIS

In this section, we analyze the performance of the proposed system model in terms of μ_ϕ . Since we focus on the impact of interference on the JSP, in what follows, we consider that at least two transmitters are located within the region of interest. Then, the following result characterizes the distances to the nearest and farthest transmitter.

Lemma 1. *Given that at least two points exist within the disc, the probability density function (PDF) of the farthest point in the disc is*

$$f_{d_k}(r) = \frac{2\lambda\pi r e^{-\lambda\pi(R^2-r^2)}}{1 - (1 + \lambda\pi R^2) e^{-\lambda\pi R^2}}, \quad r \geq 0, k \geq 2. \quad (10)$$

while, the PDF of the nearest point in the disc is as follows:

$$f_{d_1}(r) = \frac{2\lambda\pi r e^{-\lambda\pi r^2}}{1 - (1 + \lambda\pi R^2) e^{-\lambda\pi R^2}}, \quad r \geq 0. \quad (11)$$

Let us recall that the JSP is defined as the joint event that $E_1^j > E_{th}$ and $Y_1^j > \beta$. Substituting the value of the harvested energy and the SIR in equation (4) we get,

$$\mu_\phi = \mathbb{P}\left(g_1^j > d_1^\alpha \left[\frac{E_{th}}{\eta\xi\tau P_t} - \sum_{k=2}^K g_k^j d_k^{-\alpha} \right], g_1^j > \beta d_1^\alpha \sum_{k=2}^K g_k^j d_k^{-\alpha} \right). \quad (12)$$

The characterization of the above is challenging since it involves the derivation of the distribution of the sum of weighted exponential terms of the form $\sum_{k=2}^K g_k^j d_k^{-\alpha}$. Thus, obtaining the closed-form expression of μ_ϕ is infeasible. Consequently, we focus on deriving the upper bound $\mu_{\phi,U}$ and the lower bound $\mu_{\phi,L}$, of μ_ϕ . The idea behind the upper and the lower bounds of the JSP is as follows. If all the interfering transmitters are placed at the farthest location d_K in the disc, then energy harvested by the typical IoT is minimum. Similarly, if all the interfering transmitters are placed at the nearest location d_1 in the disc, then the energy harvested by the typical IoT is maximum. Let $E_1^{j,min}$ and $E_1^{j,max}$ denote the minimum and maximum harvested energy respectively. With the help of (1), we can write them as follows:

$$E_1^{j,min} = \eta\xi\tau P_t \left(g_1^j d_1^{-\alpha} + d_K^{-\alpha} \sum_{k=2}^K g_k^j \right). \quad (13)$$

$$E_1^{j,max} = \eta\xi\tau P_t \left(g_1^j d_1^{-\alpha} + d_1^{-\alpha} \sum_{k=2}^K g_k^j \right). \quad (14)$$

where E_1^j is energy harvested by s_1 node in $\xi\tau$ time, which is then used to keep s_1 node active such that it is able to read the desired transmitted signal from r_1 to s_1 in the remaining $(1-\xi)\tau$ time. Similarly, if all the interfering transmitters are placed in the same circumference as the signal transmitter i.e., at the nearest distance d_1 to the typical IoT, then this causes maximum interference to the typical IoT, hence SIR experienced by it is minimum and vice versa, as clear from the expression of SIR,

$$\Upsilon_1^{j,min} = \frac{P_t g_1^j d_1^{-\alpha}}{d_1^{-\alpha} \sum_{k=2}^K P_t g_k^j}. \quad (15)$$

$$\Upsilon_1^{j,max} = \frac{P_t g_1^j d_1^{-\alpha}}{d_K^{-\alpha} \sum_{k=2}^K P_t g_k^j}. \quad (16)$$

Case A: $Pr < Pr_{min}$.

Accordingly, we can write $\mu_{\phi,L}$ and $\mu_{\phi,U}$ as $\mu_{\phi,L} = \mathbb{P}[(E_1^j > E_{th}), (\Upsilon_1^{j,min} > \beta)] = 0$ and $\mu_{\phi,U} = \mathbb{P}[(E_1^j > E_{th}), (\Upsilon_1^{j,max} > \beta)] = 0$.

Case B: $Pr_{min} < Pr < Pr_{max}$.

Accordingly, we can write $\mu_{\phi,L}$ and $\mu_{\phi,U}$ as $\mu_{\phi,L} = \mathbb{P}[(E_1^{j,min} > E_{th}), (\Upsilon_1^{j,min} > \beta)]$ and $\mu_{\phi,U} = \mathbb{P}[(E_1^{j,max} > E_{th}), (\Upsilon_1^{j,max} > \beta)]$. The analytical expression of $\mu_{\phi,L}$ and $\mu_{\phi,U}$ are given in Theorem 1 and Theorem 2, respectively.

Theorem 1. *The lower bound of μ_ϕ is given by*

$$\begin{aligned} \mu_{\phi,L} = & \sum_{k=2}^{\infty} \left[\int_{d_1=0}^R \int_{d_K=d_1}^R \int_{z=0}^{\frac{E_{th}}{\eta\xi\tau P_t(\beta d_K^{-\alpha} + d_1^{-\alpha})}} \left(\frac{z^{k-1}}{(k-1)!} \right) \exp\left(\frac{-E_{th} d_1^{\alpha}}{\eta\xi\tau P_t} \right) \right. \\ & \left. + d_1^{\alpha} d_K^{-\alpha} z - z \right] f_{d_1}(r) f_{d_K}(r) f_K(k) d_z d_{d_K} d_{d_1} + \\ & \sum_{k=2}^{\infty} \left[\int_{d_1=0}^R \int_{d_K=d_1}^R \int_{z=\frac{E_{th}}{\eta\xi\tau P_t(\beta d_1^{-\alpha} + d_K^{-\alpha})}}^{\infty} \left(\frac{z^{k-1}}{(k-1)!} \right) \right. \end{aligned}$$

$$\left. \exp(-\beta z - z) f_{d_1}(r) f_{d_K}(r) f_K(k) \right] d_z d_{d_K} d_{d_1}, \quad (17)$$

where $f_K(k) = \frac{e^{-\lambda\pi R^2} (\lambda\pi R^2)^k}{k!}$ and $f_{d_1}(r)$ and $f_{d_K}(r)$ are obtained from (11) and (10).

Proof. A detailed proof is given in Appendix A. \square

Theorem 2. *The upper bound of μ_ϕ is given by*

$$\begin{aligned} \mu_{\phi,U} = & \sum_{k=2}^{\infty} \left[\int_{d_1=0}^R \int_{d_K=d_1}^R \int_{z=0}^{\frac{E_{th}}{\eta\xi\tau P_t(\beta d_K^{-\alpha} + d_1^{-\alpha})}} \left(\frac{z^{k-1}}{(k-1)!} \right) \right. \\ & \left. \exp\left(\frac{-E_{th} d_1^{\alpha}}{\eta\xi\tau P_t} \right) f_{d_1}(r) f_{d_K}(r) f_K(k) \right] d_z d_{d_K} d_{d_1} + \\ & \sum_{k=2}^{\infty} \left[\int_{d_1=0}^R \int_{d_K=d_1}^R \int_{z=\frac{E_{th}}{\eta\xi\tau P_t(\beta d_K^{-\alpha} + d_1^{-\alpha})}}^{\infty} \left(\frac{z^{k-1}}{(k-1)!} \right) \right. \\ & \left. \exp(-\beta d_1^{\alpha} d_K^{-\alpha} z - z) f_{d_1}(r) f_{d_K}(r) f_K(k) \right] d_z d_{d_K} d_{d_1}, \quad (18) \end{aligned}$$

where, $f_K(k) = \frac{e^{-\lambda\pi R^2} (\lambda\pi R^2)^k}{k!}$ and $f_{d_1}(r)$ and $f_{d_K}(r)$ are obtained from (11) and (10).

Proof. A detailed proof is given in Appendix B. \square

Case C: $Pr_{max} < Pr$.

Theorem 3. *The lower bound of μ_ϕ is given by*

$$\begin{aligned} \mu_{\phi,L} = & \sum_{k=2}^{\infty} \int_{d_1=0}^R \int_{z=0}^{\frac{E_{th} d_1^{\alpha}}{\eta\xi\tau P_t(1+\beta)}} \frac{z^{k-1}}{(k-1)!} \exp\left(- \left[\frac{E_{th} d_1^{\alpha}}{\eta\xi\tau P_t} \right] \right) \\ & f_{d_1}(r) f_K(k) d_z d_{d_1} + \sum_{k=2}^{\infty} \int_{d_1=0}^R \int_{z=\frac{E_{th} d_1^{\alpha}}{\eta\xi\tau P_t(1+\beta)}}^{\infty} \frac{z^{k-1}}{(k-1)!} \\ & \exp(-(\beta+1)z) f_{d_1}(r) f_K(k) d_z d_{d_1} \quad (19) \end{aligned}$$

where $f_K(k) = \frac{e^{-\lambda\pi R^2} (\lambda\pi R^2)^k}{k!}$ and $f_{d_1}(r)$ and $f_{d_K}(r)$ are obtained from (11) and (10).

Proof. A detailed proof is given in Appendix C. \square

The upper bound of μ_ϕ , ($\mu_{\phi,U}$) is same as Theorem 2.

IV. PAOI ANALYSIS

The JSP influences the PAOI since it directly characterizes the probability of success or failure in a given time slot. Recall that for the non-preemptive scenario, newly arriving packets at the transmitter are dropped until the one in transmission is successfully delivered. Based on the derived framework for JSP, the following Theorem characterizes an upper bound of the PAOI of the system.

Theorem 4. *The upper bound of the PAOI measured at the typical IoT device is*

$$A_{i,NP}^U = Z_a + \frac{2}{\mu_{\phi,L}}, \quad (20)$$

where lower bound of μ_ϕ gives an upper bound of the PAOI.

Proof. A detailed proof is given in Appendix D. \square

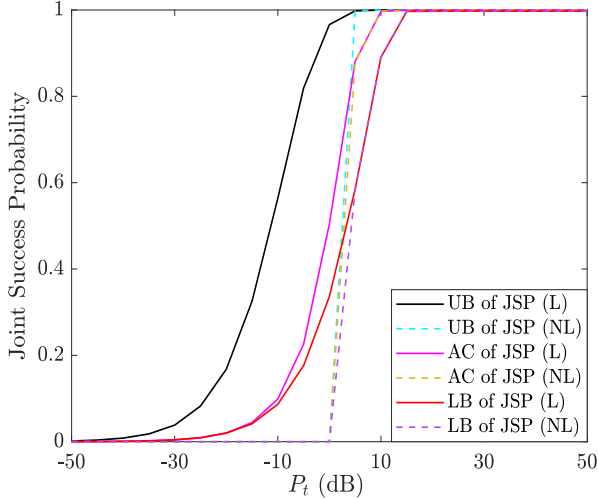


Fig. 4. The accuracy of the upper bound (UB), actual case (AC) and lower bound (LB) of the JSP, μ_ϕ for both linear energy harvesting (L EH) and NL EH models with respect to the transmit power.

Theorem 5. *The upper bound of the PAoI measured at the typical IoT device is*

$$A_{i,P}^U = Z_a + \frac{1}{\mu_{\phi,L}} + \frac{1}{q_s}, \quad (21)$$

where lower bound of μ_ϕ gives an upper bound of the PAoI and $q_s = \mu_{\phi,L} + p_a(1 - \mu_{\phi,L})$.

Proof. A detailed proof is given in Appendix E. \square

We are interested in the upper bound of PAoI since the PAoI measures the maximum time elapsed since the last received packet at the destination was generated, just before a new packet is received at the destination. This gives a guarantee on the PAoI of the system. In the next section, first, we validate and study the trends of the JSP and then investigate the optimal slot partitioning factor to optimize either the JSP or the PAoI.

V. SIMULATION RESULTS

In this section, we present simulation results to verify the derived expressions. Throughout this section, unless otherwise specified, we consider the system parameters as $E_{th} = 10$ mJ, $\alpha = 3$, $\sigma = 10$ bits, $\eta = 0.9$, $\xi = 0.4$, $\tau = 1$ sec, $\lambda = 0.003$ m⁻², $R = 60$ m, $B = 10$ kHz.

A wide range of bandwidths, from a few kHz to several GHz, can be utilized by IoT devices, contingent upon their applications and specifications. IoT devices with low bandwidth operate within the kHz range, making them ideal for low-power communication e.g., AM/FM radio that involves the transmission of minimal data in the range of a few Kbps using protocols like LoRaWAN and Zigbee. Medium-bandwidth IoT devices operate within the range of a few MHz, so moderate data transmission in the Mbps range can be used for real-time monitoring and control through protocols like Bluetooth and LTE-M.

According to the L EH model as shown by the dashed lines in Fig. 4, the actual value of JSP matches the LB for lower transmit power values and the UB for higher transmit power

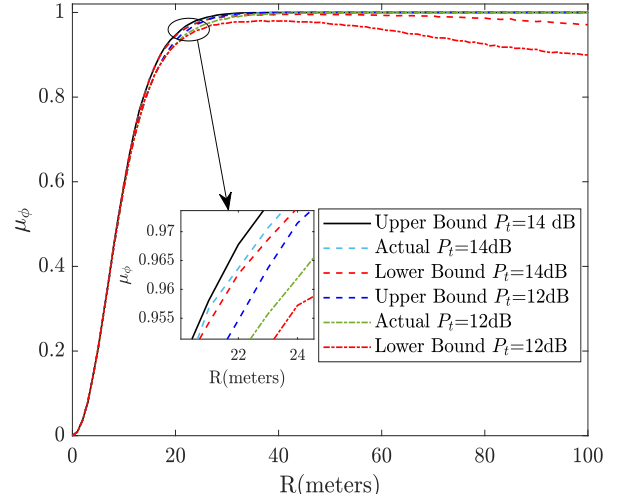


Fig. 5. Lower and upper bounds of joint success probability, μ_ϕ with respect to the radius, R compared with the actual simulation when received power P_r lies in between $P_{r,min}$ and $P_{r,max}$.

values. On the contrary, we see from Fig. 5 that for a varied range of deployment areas, the lower and the upper bounds closely follow the actual JSP. The JSP monotonically increases with the transmit power. This is because, with an increase in P_t , the EH increases, while it has no impact on the SIR, where P_t appears both in the numerator and the denominator, and hence cancels out. Interestingly, with an increase of R the JSP first increases, reaches an optimal value and then decreases further. The initial increase is due to the enhancement in the EH caused by an increase in the number of transmitters. Albeit, this deteriorates the SIR, but for lower values of R , the SIR already exceeds its corresponding threshold. On the contrary, for larger values of R , the SIR deteriorates due to an increase in the number of interferers.

NL EH as shown by dotted lines in Fig. 4 and Fig. 10 embodies a real-world scenario, as it simulates a realistic system where power constraints (both minimum and maximum) are imposed; specifically, no energy is harvested below a designated power threshold, and there exists a limit on the maximum EH, which is essential in practical energy-harvesting systems.

The plots of both figures, for the L EH and NL EH models, overlap at higher power levels, but separate at lower power levels. At low power levels, the plots diverge due to the NL EH scenario, which establishes a minimum power threshold $P_{r,min}$ beneath which energy cannot be harvested. This results in a significant decline in JSP and consequently the ξ^* for maximizing the lower bound of JSP, whereas in the L EH scenario, the IoT continues to harvest energy linearly, yielding higher JSP. At higher power levels, both scenarios yield similar JSP values, as in the non linear (NL) case, EH saturates at $P_{r,max}$, whereas in the linear (L) case, EH increases linearly with power and the EH, both capped and uncapped are large enough to exceed the energy threshold, E_{th} also the SIR condition is readily fulfilled.

L EH model as shown by dashed lines in Fig. 6 and Fig.7 confirm that even at small values of ξ , some energy

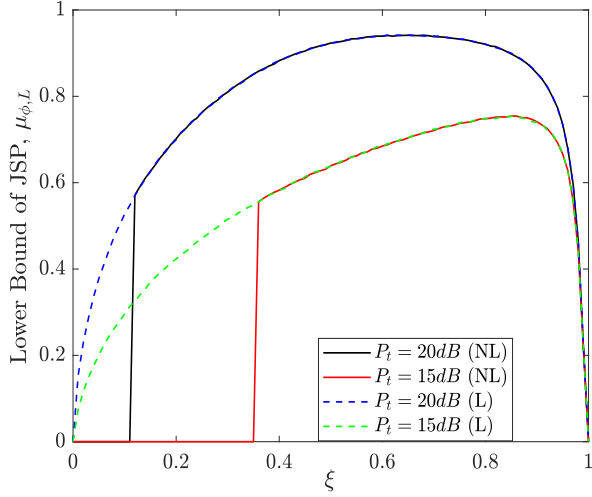


Fig. 6. Lower bound of joint success probability, $\mu_{\phi,L}$ with respect to fraction of time slot, ξ for radius = 50 m.

is still harvested, albeit small. As ξ increases, the EH also increases, and the probability of meeting both the energy and SIR thresholds improves. Therefore, the JSP curve will likely increase smoothly while PAoI will likely decrease smoothly since, there is no cap on the harvested energy. The Fig. 7 also illustrates that the PAoI for the preemptive queue discipline is consistently lower than that of the non-preemptive queue discipline for all values of the time slot fraction, ξ . This outcome proves that the preemptive queue discipline outperforms the non-preemptive approach. As ξ further increases, despite higher energy harvesting, the overall JSP declines because the system fails to meet the SIR requirement due to insufficient transmission time. This trade-off between energy harvesting and data transmission time results in the JSP curve declining as ξ approaches 1. In other words, when ξ is small, the IoT device does not harvest sufficient energy to be able to successfully decode the data packets in the data transmission phase, resulting in lower $\mu_{\phi,L}$, higher $A_{i,NP}^U$ and higher $A_{i,P}^U$ respectively. Similarly, when ξ is large, the data transmission interval is low, resulting in a higher link rate requirement. This degrades $\mu_{\phi,L}$, $A_{i,NP}^U$ and $A_{i,P}^U$ respectively. This establishes the existence of an optimal slot partitioning factor ξ^* that maximizes JSP and minimizes PAoI, for a disc of a given radius, corresponding to each value of transmit power. This is clearly demonstrated in Fig. 8 for discs of varying radii, where we can also observe that as the power transmitted increases, EH also increases; thus, to further increase the maximum possible JSP, greater time can be allotted to information decoding, thereby decreasing ξ^* . In conclusion, ξ^* for lower values of transmit power are always greater than ξ^* values for higher values of transmit power.

In NL EH model, as shown by dotted lines in Fig. 6 and Fig.7. At low ξ , if the received power P_r is below the $P_{r,min}$ threshold, then no energy is harvested. This can result in a sharper decline or a flat region in the JSP and PAoI plot, due to the energy constraint not being met. Once P_r exceeds $P_{r,min}$, energy harvesting starts and JSP will increase and PAoI will decrease, but at a slower rate due to the conditions and caps

imposed on P_r . When the received power exceeds $P_{r,max}$, the energy is capped, meaning that even with a further increase in ξ , the energy harvesting no longer increases linearly. This results in the JSP and PAoI curve flattening at high ξ values. As ξ increases further, more time is spent harvesting energy and less time is available for data transmission. This reduction in available time for transmitting data negatively impacts the system's ability to meet the SIR requirement. Specifically, the threshold for the SIR, represented by β increases as ξ increases because the available time for transmission becomes smaller. As ξ approaches 1, the transmission time $(1 - \xi)$ becomes close to zero, making it harder to meet the SIR threshold, and thus reducing the JSP and increase PAoI. While more energy is harvested at high ξ , the benefit of increased energy is offset by the decreasing transmission time and the increasing SIR threshold β . Essentially, while the system might have sufficient energy, the data transmission reliability deteriorates, and the likelihood of successful joint energy harvesting and data transmission declines.

From (20), we see that the term $Z_a = \left(\frac{1}{p_a} - 1\right)$ is independent of ξ so $A_{i,NP}^U$ is minimized and $\mu_{\phi,L}$ is maximized for the same optimal ξ . Upon differentiating (21) i.e. $A_{i,P}^U$ with respect to $\mu_{\phi,L}$, we get, $\frac{dA_{i,P}^U}{d\mu_{\phi,L}} = -\frac{1}{\mu_{\phi,L}^2} - \frac{(1-p_a)}{(\mu_{\phi,L} + p_a(1-\mu_{\phi,L}))^2} < 0$ for the range $p_a \in [0, 1]$. This means that $A_{i,P}^U$ is monotonically decreasing with respect to $\mu_{\phi,L}$ so $A_{i,P}^U$ is minimized simultaneously when $\mu_{\phi,L}$ is maximized for the same optimal ξ . Thus we conclude that $\mu_{\phi,L}$ is maximized while $A_{i,P}^U$, $A_{i,NP}^U$ are minimized for the same value of ξ^* which is represented in Fig. 8. Here we can also observe that the optimal ξ plots for maximizing JSP are the same as the optimal ξ plots for minimizing PAoI where the actual case plots lie in between the upper and lower bound plots. Another observation here is that as the radius increases, the plots of the bounds get farther away from each other and also from the actual case in a peculiar way that encompasses the crossing of the $R = 50$ m and $R = 200$ m plots of ξ^* for maximizing the lower bound of JSP and minimizing the upper bound of PAoI. This is explained by Fig. 9, L EH model as follows.

Fig. 9, L EH model shows that when the transmit power is low, say $P_t = 5$ dB and the radius is very small, the number of interfering transmitters is also very less and barely grows with a small increase in the radius. At the same time, the signaling transmitter is very close to the receiver, so the $SIR > \beta$ threshold condition is easily met and the IoT device also harvests a small amount of energy, enough to meet the threshold, $EH > E_{th}$. However, with a small increase in the radius, the amount of energy harvested drops, therefore, EH time has to be increased by increasing ξ^* which maximizes JSP and minimizes PAoI.

At higher R values, as R increases, the number of interference transmitters increases significantly. This means that excessive interference and insufficient signal power collectively hinder signal decoding, which in turn lowers the SIR. Thus, in order to maximize JSP and minimize PAoI, more time must be allocated for signal decoding, by decreasing ξ^* .

When the transmit power is high, say $P_t = 20$ dB and the radius is very small then with a small increase in the

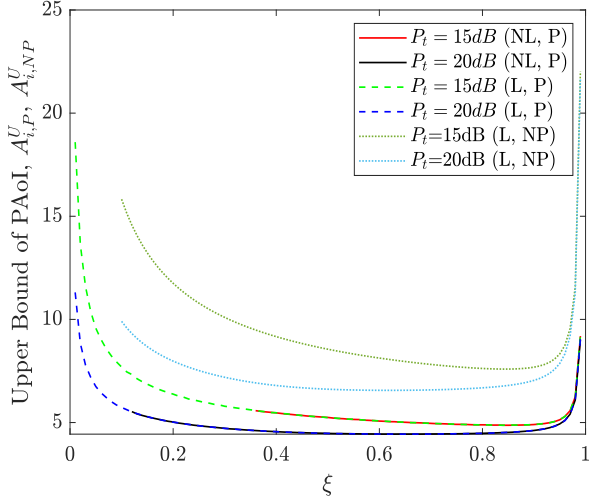


Fig. 7. Upper Bound of PAoI under both preemptive and non-preemptive queuing disciplines, $A_{i,P}^U, A_{i,NP}^U$ with respect to fraction of time slot, ξ .

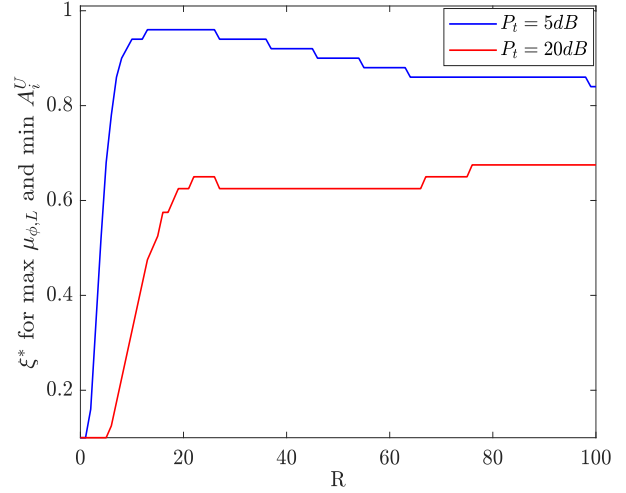


Fig. 9. Optimal slot partitioning, ξ^* for maximizing lower bound of JSP, $\mu_{\phi,L}$ and minimizing upper bounds of PAoI, $A_{i,P}^U, A_{i,NP}^U$ with respect to radius, R .

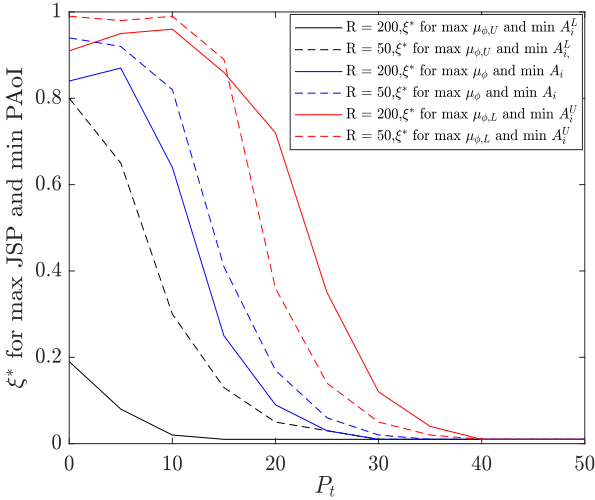


Fig. 8. Optimal slot partitioning, ξ^* for maximizing upper $\mu_{\phi,U}$, actual μ_{ϕ} and lower $\mu_{\phi,L}$ bounds of joint success probability and minimizing lower $A_{i,P}^L, A_{i,NP}^L$, actual $A_{i,P}, A_{i,NP}$ and upper $A_{i,P}^U, A_{i,NP}^U$ bounds of PAoI, with respect to transmit power, P_t in L EH model.

radius, ξ^* is increased for the same reason as previously stated; however, for larger R values, as R increases, the number of interferers increase significantly. Since stronger transmit power overcomes interference more efficiently, so the decrease in the SIR is not enough to hamper signal decoding, hence, more energy can be harvested by increasing ξ^* to further maximize JSP. This ensures that even with lesser time available for data transmission, the transmissions are successful a lot more often. This efficient use of higher transmit power allows JSP for higher values of radius to be greater than JSP for lower values of radius.

A really interesting observation in Fig. 8 in the L EH model in the actual case plot drawn for different R values is that, as the radius of the disc increases, the number of interferers increase significantly, thus decreasing SIR so the

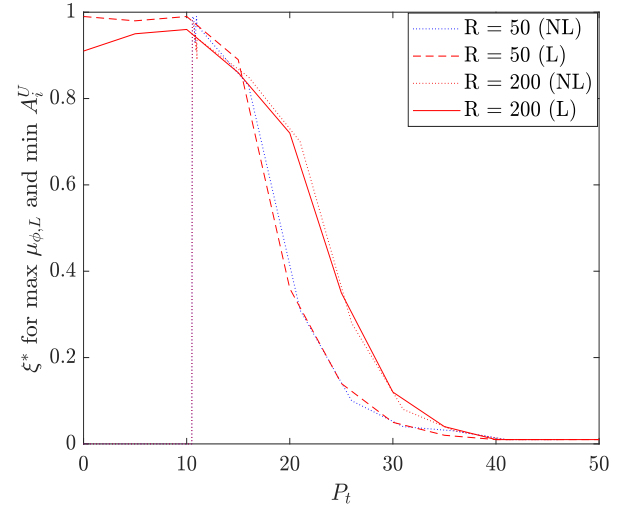


Fig. 10. Optimal slot partitioning, ξ^* for maximizing lower bound of joint success probability, $\mu_{\phi,L}$ and minimizing upper bound of PAoI, $A_{i,P}^U, A_{i,NP}^U$ with respect to transmit power, P_t in both L EH and NL EH model.

signal decoding time needs to be increased by decreasing the optimum charging phase duration, ξ^* in order to maximize JSP for all values of transmit power, P_t .

One clear distinction between the plots of the upper bound and the actual case of ξ^* for minimizing PAoI in Fig. 8 is that, in the upper bound plot, at lower values of transmit power, P_t and in the actual case plot, at all values of power transmitted by the signaling transmitter, as the radius increases, the number of interferers increase significantly, thereby increasing interference. As a result, signal decoding time at IoT must be increased by decreasing the ξ^* .

On the contrary, we can see in the plot of the upper bound of ξ^* for minimizing PAoI that, at higher values of transmit power, as the radius increases, so does the ξ^* . This occurs in the boundary case because higher transmit power values overcome interference more efficiently. As a result, IoT can

leverage this situation to maximize JSP by increasing ξ^* . By increasing the ξ^* , IoT can harvest more energy, allowing signal decoding to improve even as signal decoding time at IoT decreases.

VI. CONCLUSION

This paper considered an IoT network where the IoT devices harvest energy from the power received from the transmitters and use it to decode the data packets. We then define and derive the lower and upper bounds for the metric JSP and the upper bound for the metric PAoI. Our analytical results show how time slot partitioning factor, deployment area, and other wireless network parameters affect JSP and PAoI. The key observations were that in NL EH, no energy is harvested below a certain power threshold, and the highest harvested energy is restricted, which is essential for the design of practical energy-harvesting systems. The preemptive queue discipline consistently outperforms the non-preemptive approach, as evidenced by the fact that the PAoI is lower for the preemptive queue discipline than for the non-preemptive queue discipline for all values of the time slot fraction, ξ . An optimal slot partitioning factor ξ^* exists that maximizes JSP and minimizes PAoI in both preemptive and non-preemptive queuing disciplines for a disc of a specific radius, corresponding to each value of transmit power. Further, we illustrate how this factor stays the same across each of the three cases. As the radius increases, the number of interferers increase, leading to increased interference, thus reducing ξ^* in the upper bound plot of ξ^* for minimizing PAoI, for only the lower values of transmit power, P_t and for all values of transmit power, P_t in the actual case plot. However, at higher values of transmit power, ξ^* grows with radius in the upper bound plot of ξ^* for minimizing PAoI, because higher transmit power values help the IoT to overcome interference more efficiently, thus maximizing JSP by increasing ξ^* despite facing a decrease in decoding time. As a promising avenue of future work, one can analyze protocols like ALOHA and CSMA-CD with a channel access parameter which can be optimized using some suitable RL algorithm.

APPENDIX A

PROOF OF THEOREM 1

The lower bound of μ_ϕ is given as follows: $\mu_{\phi,L} = \mathbb{P}[(E_1^{j,min} > E_{th}), (\Upsilon_1^{j,min} > \beta)]$. Using (13) and (15), we can write $\mu_{\phi,L}$ as

$$\begin{aligned} \mu_{\phi,L} &= \mathbb{P}\left(g_1^j > \underbrace{d_1^\alpha \left[\frac{E_{th}}{\eta\xi\tau P_t} - d_K^{-\alpha} \sum_{k=2}^K g_k^j \right]}_{\Theta_1}, g_1^j > \beta \underbrace{\sum_{k=2}^K g_k^j}_{\Theta_2}\right) \\ &= \mathbb{P}(g_1^j > \max(\Theta_1, \Theta_2)) \\ &= \underbrace{\mathbb{P}(g_1^j > \Theta_1, \Theta_1 > \Theta_2)}_{R_1} + \underbrace{\mathbb{P}(g_1^j > \Theta_2, \Theta_2 > \Theta_1)}_{R_2} \quad (22) \end{aligned}$$

In the above expression, there are two probabilities that need to be solved. We solve them one by one. If $\Theta_1 > \Theta_2$, then we have $[E_{th}/\eta\xi\tau P_t - d_K^{-\alpha} Z] > \beta d_1^{-\alpha} Z$, where $Z = \sum_{k=2}^K g_k^j$.

To solve R_1 , we have

$$R_1 = \mathbb{P}\left(g_1^j > d_1^\alpha \left[\frac{E_{th}}{\eta\xi\tau P_t} - Z d_K^{-\alpha} \right], Z < \frac{E_{th}}{\eta\xi\tau P_t [\beta d_1^{-\alpha} + d_K^{-\alpha}]}\right) \quad (23)$$

Let $t = d_1^\alpha \left[\frac{E_{th}}{\eta\xi\tau P_t} - Z d_K^{-\alpha} \right]$. If $t \geq 0 \Rightarrow Z \leq \frac{E_{th} d_K^\alpha}{\eta\xi\tau P_t}$. If $t < 0 \Rightarrow Z > \frac{E_{th} d_K^\alpha}{\eta\xi\tau P_t}$. The condition $t < 0$ will not occur since channel fading cannot be negative. Hence, we have

$$R_1 = \mathbb{P}\left(g_1^j > t, t > 0, Z < \frac{E_{th}}{\eta\xi\tau P_t [\beta d_1^{-\alpha} + d_K^{-\alpha}]}\right) \quad (24)$$

On substituting $t = d_1^\alpha \left[\frac{E_{th}}{\eta\xi\tau P_t} - Z d_K^{-\alpha} \right]$, we have

$$\begin{aligned} R_1 &= \mathbb{P}\left(g_1^j > d_1^\alpha \left[\frac{E_{th}}{\eta\xi\tau P_t} - Z d_K^{-\alpha} \right], \right. \\ &\quad \left. Z < \min\left(\frac{E_{th}}{\eta\xi\tau P_t [\beta d_1^{-\alpha} + d_K^{-\alpha}]}, \frac{E_{th} d_K^\alpha}{\eta\xi\tau P_t}\right)\right) \quad (25) \end{aligned}$$

Since, $\frac{E_{th}}{\eta\xi\tau P_t [\beta d_1^{-\alpha} + d_K^{-\alpha}]}$ is always less than $\frac{E_{th} d_K^\alpha}{\eta\xi\tau P_t}$. We can write

$$\begin{aligned} R_1 &= \mathbb{P}\left(g_1^j > d_1^\alpha \left[\frac{E_{th}}{\eta\xi\tau P_t} - Z d_K^{-\alpha} \right], Z < \frac{E_{th}}{\eta\xi\tau P_t [\beta d_1^{-\alpha} + d_K^{-\alpha}]}\right) \\ &= \mathbb{E}_Z \left\{ \exp\left(-d_1^\alpha \left[\frac{E_{th}}{\eta\xi\tau P_t} - Z d_K^{-\alpha} \right], Z < \frac{E_{th}}{\eta\xi\tau P_t [\beta d_1^{-\alpha} + d_K^{-\alpha}]}\right) \right\} \\ &= \int_0^{\frac{E_{th}}{\eta\xi\tau P_t [\beta d_1^{-\alpha} + d_K^{-\alpha}]}} \exp\left(-d_1^\alpha \left[\frac{E_{th}}{\eta\xi\tau P_t} - Z d_K^{-\alpha} \right]\right) f_Z(Z) dZ \quad (26) \end{aligned}$$

The PDF of Z , $f_Z(Z)$ is as follows: $f_Z(Z) = \frac{e^{-Z} Z^{k-1}}{(k-1)!}$. Using $f_Z(Z)$ in(26), we get

$$\begin{aligned} R_1 &= \int_0^{\frac{E_{th}}{\eta\xi\tau P_t [\beta d_1^{-\alpha} + d_K^{-\alpha}]}} \frac{Z^{k-1}}{(k-1)!} \\ &\quad \exp\left(-\left[\frac{E_{th} d_1^\alpha}{\eta\xi\tau P_t} - Z d_1^\alpha d_K^{-\alpha} + Z\right]\right) dZ \quad (27) \end{aligned}$$

To Solve R_2 , we can write

$$\begin{aligned} R_2 &= \mathbb{P}\left(g_1^j > \beta Z, Z < \frac{E_{th}}{\eta\xi\tau P_t [\beta d_1^{-\alpha} + d_K^{-\alpha}]}\right) \\ &= \mathbb{E}_Z \left\{ \exp(-\beta Z), Z > \frac{E_{th}}{\eta\xi\tau P_t (\beta d_1^{-\alpha} + d_K^{-\alpha})} \right\} \quad (28) \\ &= \int_{\frac{E_{th}}{\eta\xi\tau P_t (\beta d_1^{-\alpha} + d_K^{-\alpha})}}^{\infty} \exp(-\beta Z) f_Z(z) dZ \end{aligned}$$

The PDF of Z , $f_Z(Z)$ is as follows: $f_Z(Z) = \frac{e^{-Z} Z^{k-1}}{(k-1)!}$. Using $f_Z(Z)$ in (28), we get

$$R_2 = \int_{\frac{E_{th}}{\eta\xi\tau P_t (\beta d_1^{-\alpha} + d_K^{-\alpha})}}^{\infty} \exp(-\beta Z - Z) \frac{Z^{k-1}}{(k-1)!} dZ \quad (29)$$

Replacing (27) and (29) in (22), we get (17).

APPENDIX B

PROOF OF THEOREM 2

Upper Bound of μ_ϕ is given as follows: $\mu_{\phi,U} = \mathbb{P}[(E_1^{j,max} > E_{th}), (\Upsilon_1^{j,max} > \beta)]$. Using (14) and (16), we can write μ_ϕ^U as

$$\begin{aligned} \mu_\phi^U &= \mathbb{P}\left(g_1^j > d_1^\alpha \underbrace{\left[\frac{E_{th}}{\eta\xi\tau P_t} - d_1^{-\alpha} \sum_{k=2}^K g_k^j\right]}_{\Theta_3}, \underbrace{g_1^j > \beta d_1^\alpha d_K^{-\alpha} \sum_{k=2}^K g_k^j}_{\Theta_4}\right) \\ &= \mathbb{P}(g_1^j > \max(\Theta_3, \Theta_4)) \\ &= \underbrace{\mathbb{P}(g_1^j > \Theta_3, \Theta_3 > \Theta_4)}_{R_3} + \underbrace{\mathbb{P}(g_1^j > \Theta_4, \Theta_4 > \Theta_3)}_{R_4}. \end{aligned} \quad (30)$$

In the above expression, there are two probabilities that need to be solved. We solve them one by one. If $\Theta_3 > \Theta_4$ then we have $\left[E_{th}/\eta\xi\tau P_t - d_1^{-\alpha} Z\right] > \beta d_K^{-\alpha} Z$, where $Z = \sum_{k=2}^K g_k^j$.

To solve R_3 , we have

$$R_3 = \mathbb{P}\left(g_1^j > d_1^\alpha \left[\frac{E_{th}}{\eta\xi\tau P_t} - Z d_1^{-\alpha}\right], Z < \frac{E_{th}}{\eta\xi\tau P_t [\beta d_K^{-\alpha} + d_1^{-\alpha}]}\right)$$

Let $t = d_1^\alpha \left[\frac{E_{th}}{\eta\xi\tau P_t} - Z d_1^{-\alpha}\right]$. If $t > 0 \Rightarrow Z < \frac{E_{th} d_1^\alpha}{\eta\xi\tau P_t}$. If $t < 0 \Rightarrow Z > \frac{E_{th} d_1^\alpha}{\eta\xi\tau P_t}$. The condition $t < 0$ will not occur since channel fading cannot be negative. Hence, we have

$$R_3 = \mathbb{P}\left(g_1^j > t, t > 0, Z < \frac{E_{th}}{\eta\xi\tau P_t [\beta d_K^{-\alpha} + d_1^{-\alpha}]}\right) \quad (31)$$

On substituting $t = d_1^\alpha \left[\frac{E_{th}}{\eta\xi\tau P_t} - Z d_1^{-\alpha}\right]$, we have

$$\begin{aligned} R_3 &= \mathbb{P}\left(g_1^j > d_1^\alpha \left[\frac{E_{th}}{\eta\xi\tau P_t} - Z d_1^{-\alpha}\right], \right. \\ &\quad \left. Z < \min\left(\frac{E_{th}}{\eta\xi\tau P_t [\beta d_K^{-\alpha} + d_1^{-\alpha}]}, \frac{E_{th} d_1^\alpha}{\eta\xi\tau P_t}\right)\right). \end{aligned}$$

Since $\frac{E_{th}}{\eta\xi\tau P_t [\beta d_K^{-\alpha} + d_1^{-\alpha}]}$ is always less than $\frac{E_{th} d_1^\alpha}{\eta\xi\tau P_t}$. We can write

$$\begin{aligned} R_3 &= \mathbb{P}\left(g_1^j > d_1^\alpha \left[\frac{E_{th}}{\eta\xi\tau P_t} - Z d_1^{-\alpha}\right], Z < \frac{E_{th}}{\eta\xi\tau P_t [\beta d_K^{-\alpha} + d_1^{-\alpha}]}\right) \\ &= \mathbb{E}_Z \left\{ \exp\left(-d_1^\alpha \left[\frac{E_{th}}{\eta\xi\tau P_t} - Z d_1^{-\alpha}\right], Z < \frac{E_{th}}{\eta\xi\tau P_t [\beta d_K^{-\alpha} + d_1^{-\alpha}]}\right) \right\} \\ &= \int_0^{\frac{E_{th}}{\eta\xi\tau P_t [\beta d_K^{-\alpha} + d_1^{-\alpha}]}} \exp\left(-d_1^\alpha \left[\frac{E_{th}}{\eta\xi\tau P_t} - Z d_1^{-\alpha}\right]\right) f_Z(Z) dZ. \end{aligned} \quad (32)$$

The PDF of Z , $f_Z(Z)$ is as follows: $f_Z(Z) = \frac{e^{-Z} Z^{k-1}}{(k-1)!}$. Using $f_Z(Z)$ in (32), we get

$$R_3 = \int_0^{\frac{E_{th}}{\eta\xi\tau P_t [\beta d_K^{-\alpha} + d_1^{-\alpha}]}} \exp\left(-\left[\frac{E_{th} d_1^\alpha}{\eta\xi\tau P_t}\right]\right) \frac{Z^{k-1}}{(k-1)!} dZ. \quad (33)$$

To Solve R_4 , we can write

$$R_4 = \mathbb{P}\left(g_1^j > \beta d_1^\alpha d_K^{-\alpha} Z, Z < \frac{E_{th}}{\eta\xi\tau P_t [\beta d_K^{-\alpha} + d_1^{-\alpha}]}\right)$$

$$\begin{aligned} &= \mathbb{E}_Z \left\{ \exp\left(-\beta d_1^\alpha d_K^{-\alpha} Z\right), Z > \frac{E_{th}}{\eta\xi\tau P_t (\beta d_K^{-\alpha} + d_1^{-\alpha})} \right\} \\ &= \int_{\frac{E_{th}}{\eta\xi\tau P_t (\beta d_K^{-\alpha} + d_1^{-\alpha})}}^{\infty} \exp\left(-\beta d_1^\alpha d_K^{-\alpha} Z\right) f_Z(z) dZ. \end{aligned} \quad (34)$$

The PDF of Z , $f_Z(Z)$ is as follows: $f_Z(Z) = \frac{e^{-Z} Z^{k-1}}{(k-1)!}$. Using $f_Z(Z)$ in (34), we get

$$R_4 = \int_{\frac{E_{th}}{\eta\xi\tau P_t (\beta d_K^{-\alpha} + d_1^{-\alpha})}}^{\infty} \exp\left(-\beta d_1^\alpha d_K^{-\alpha} Z - Z\right) \frac{Z^{k-1}}{(k-1)!} dZ. \quad (35)$$

Replacing (33) and (35) in (30), we get, (18)

APPENDIX C PROOF OF THEOREM 3

The lower bound of μ_ϕ is given as follows: $\mu_{\phi,L} = \mathbb{P}[(E_1^j > E_{th}), (\Upsilon_1^{j,min} > \beta)]$. Using (2) and (15), we can write $\mu_{\phi,L}$ as

$$\begin{aligned} \mu_{\phi,L} &= P \left[g_1^j > d_1^\alpha \underbrace{\left(\frac{E_{th}}{\eta\xi\tau P_t} - d_1^{-\alpha} \sum_{k=2}^K g_k^j\right)}_{\Theta_5}, \underbrace{g_1^j > \beta \sum_{k=2}^K g_k^j}_{\Theta_6} \right] \\ &= P \left[g_1^j > \max(\Theta_5, \Theta_6) \right] \\ &= \underbrace{\mathbb{P}\left(g_1^j > \Theta_5, \Theta_5 > \Theta_6\right)}_{R_5} + \underbrace{\mathbb{P}\left(g_1^j > \Theta_6, \Theta_6 > \Theta_5\right)}_{R_6} \end{aligned} \quad (36)$$

In the above expression, there are two probabilities that need to be solved. We solve them one by one. If $\Theta_5 > \Theta_6$, then we have $d_1^\alpha \left(\frac{E_{th}}{\eta\xi\tau P_t} - d_1^{-\alpha} Z\right) > \beta Z$ where $Z = \sum_{k=2}^K g_k^j$. To solve R_5 , we have

$$R_5 = \mathbb{P}\left(g_1^j > d_1^\alpha \left(\frac{E_{th}}{\eta\xi\tau P_t} - d_1^{-\alpha} Z\right), Z < \frac{E_{th} d_1^\alpha}{\eta\xi\tau P_t (1 + \beta)}\right) \quad (37)$$

Let $t = d_1^\alpha \left(\frac{E_{th}}{\eta\xi\tau P_t} - d_1^{-\alpha} Z\right)$. If $t \geq 0 \Rightarrow Z < \frac{E_{th} d_1^\alpha}{\eta\xi\tau P_t}$. If $t < 0 \Rightarrow Z > \frac{E_{th} d_1^\alpha}{\eta\xi\tau P_t}$. The condition $t < 0$ will not occur since channel fading cannot be negative. Hence we have

$$R_5 = \mathbb{P}\left(g_1^j > t, t > 0, Z < \frac{E_{th} d_1^\alpha}{\eta\xi\tau P_t (1 + \beta)}\right) \quad (38)$$

On substituting $t = d_1^\alpha \left(\frac{E_{th}}{\eta\xi\tau P_t} - d_1^{-\alpha} Z\right)$, we have

$$\begin{aligned} R_5 &= \mathbb{P}\left(g_1^j > d_1^\alpha \left[\frac{E_{th}}{\eta\xi\tau P_t} - d_1^{-\alpha} Z\right], Z < \min\left(\frac{E_{th} d_1^\alpha}{\eta\xi\tau P_t}, \frac{E_{th} d_1^\alpha}{\eta\xi\tau P_t (1 + \beta)}\right)\right) \\ &= \mathbb{P}\left(g_1^j > d_1^\alpha \left[\frac{E_{th}}{\eta\xi\tau P_t} - d_1^{-\alpha} Z\right], Z < \frac{E_{th} d_1^\alpha}{\eta\xi\tau P_t (1 + \beta)}\right) \\ &= \mathbb{E}_Z \left\{ \exp\left(-d_1^\alpha \left[\frac{E_{th}}{\eta\xi\tau P_t} - d_1^{-\alpha} Z\right], Z < \frac{E_{th} d_1^\alpha}{\eta\xi\tau P_t (1 + \beta)}\right) \right\} \\ &= \int_{z=0}^{\frac{E_{th} d_1^\alpha}{\eta\xi\tau P_t (1 + \beta)}} \exp\left(-d_1^\alpha \left[\frac{E_{th}}{\eta\xi\tau P_t} - d_1^{-\alpha} Z\right]\right) f_Z(z) dz \end{aligned} \quad (39)$$

The PDF of Z , $f_Z(Z)$ is as follows: $f_Z(Z) = \frac{e^{-Z} Z^{k-1}}{(k-1)!}$. Using $f_Z(Z)$ in (39), we get

$$R_5 = \int_{z=0}^{\frac{E_{th} d_1^\alpha}{\eta \xi \tau P_t (1+\beta)}} \frac{Z^{k-1}}{(k-1)!} \exp\left(-\left[\frac{E_{th} d_1^\alpha}{\eta \xi \tau P_t}\right]\right) dz \quad (40)$$

To solve R_6 , we can write

$$\begin{aligned} R_6 &= \mathbb{P}\left[g_1^j > \beta Z, Z > \frac{E_{th} d_1^\alpha}{\eta \xi \tau P_t (1+\beta)}\right] \\ &= \mathbb{E}_Z \left\{ \exp(-\beta Z), Z > \frac{E_{th} d_1^\alpha}{\eta \xi \tau P_t (1+\beta)} \right\} \\ &= \int_{z=\frac{E_{th} d_1^\alpha}{\eta \xi \tau P_t (1+\beta)}}^{\infty} \exp(-\beta Z) f_Z(z) dz \end{aligned} \quad (41)$$

The PDF of Z , $f_Z(Z)$ is as follows: $f_Z(Z) = \frac{e^{-Z} Z^{k-1}}{(k-1)!}$. Using $f_Z(Z)$ in (41), we get

$$R_6 = \int_{z=\frac{E_{th} d_1^\alpha}{\eta \xi \tau P_t (1+\beta)}}^{\infty} \frac{Z^{k-1}}{(k-1)!} \exp(-(\beta+1)Z) dz \quad (42)$$

Replacing (40) and (42) in (36), we get (19)

APPENDIX D PROOF OF THEOREM 4

We can obtain $\mathbb{E}[W_i] = \sum_{n=1}^{\infty} n [\mu_{\phi,L} (1 - \mu_{\phi,L})^{n-1}]$.

Replacing $1 - \mu_{\phi,L} = t$, we get,

$$\mathbb{E}[W_i] = \sum_{n=1}^{\infty} n (1-t) t^{n-1} = \frac{1}{1-t} = \frac{1}{\mu_{\phi,L}}. \quad (43)$$

Similarly for V_i we can obtain $\mathbb{E}[V_i] = \sum_{n=0}^{\infty} n [p_a (1-p_a)^n]$. Replacing $1 - p_a = w$, we get,

$$\mathbb{E}[V_i] = \sum_{n=0}^{\infty} n (1-w) w^n = \frac{w}{1-w} \approx Z_a, \quad (44)$$

Thus, the upper bound of PAoI measured at the typical IoT is given by $A_{i,NP}^U = \mathbb{E}[A_i | (\beta, E_{th}) : \phi]$. From (6) and (7), $A_{i,NP}^U = \mathbb{E}[W_{i-1}] + \mathbb{E}[V_i] + \mathbb{E}[W_i]$. From (43) and (44), we get (20).

APPENDIX E PROOF OF THEOREM 5

There are $N_i = n$ packet arrivals in $(s-m)$ slots and no packet arrivals in m slots.

$$\begin{aligned} \mathbb{P}[\hat{W}_i = m / W_i = s] &= \mathbb{P}[N_i = n \text{ packet arrivals in } (s-m) \text{ slots}] \\ &\quad * \mathbb{P}[\text{no packet arrivals in } m \text{ slots}] \\ &= \sum_{n=0}^{s-m} \mathbb{P}[X_n] * (1-p_a)^m \end{aligned} \quad (45)$$

We want to know the number of trials $(s-m)$ required to achieve a fixed number of successfully arrived replacement

packets, n , where, $n=0$ to $(s-m)$, using negative binomial distribution we get,

$$= \sum_{n=0}^{s-m} \binom{(s-m)-1}{n-1} p_a^n (1-p_a)^{(s-m)-n} * (1-p_a)^m \quad (46)$$

Putting $n=1$ because we have at least one arrived packet that is being serviced in the consecutive time slots gives,

$$= \begin{cases} p_a & , (s=1) \\ \sum_{n=1}^{(s-m)+1} \binom{(s-m)}{n-1} p_a^n (1-p_a)^{s-n} & , (s \geq m > 1) \\ (1-p_a)^{m-1} & , (s=m) \end{cases} \quad (47)$$

PMF of \hat{W}_i is as follows:

$$\begin{aligned} \mathbb{P}[\hat{W}_i = m] &= \sum_{s=m}^{\infty} \mathbb{P}[\hat{W}_i = m / W_i = s] \mathbb{P}[W_i = s] \\ &= \mathbb{P}[\hat{W}_i = m / W_i = m] \mathbb{P}[W_i = m] + \\ &\quad \sum_{s=m+1}^{\infty} \mathbb{P}[\hat{W}_i = m / W_i = s] \mathbb{P}[W_i = s] \\ &= (1-p_a)^{m-1} \mu_{\phi,L} (1-\mu_{\phi,L})^{m-1} + \\ &\quad \underbrace{\sum_{n=1}^{(s-m)+1} \binom{(s-m)}{n-1} p_a^n (1-p_a)^{s-n} \sum_{s=m+1}^{\infty} \mu_{\phi,L} (1-\mu_{\phi,L})^{s-1}}_G \end{aligned} \quad (48)$$

Substituting $s-m=l$ in the above term G we get,

$$G = \sum_{n=1}^{l+1} \binom{l}{n-1} p_a^n (1-p_a)^{l+m-n} \sum_{l=1}^{\infty} \mu_{\phi,L} (1-\mu_{\phi,L})^{l+m-1} \quad (49)$$

Put $l+1=z$ and $n=1$, we get,

$$G = p_a (1-p_a)^{m-1} \mu_{\phi,L} (1-\mu_{\phi,L})^m \sum_{z=2}^{\infty} (1-\mu_{\phi,L})^{z-2} \quad (50)$$

Put $z-2=a$ and $\sum_{a=0}^{\infty} x^a = \frac{1}{1-x}$ for $|x| < 1$

$$G = p_a (1-p_a)^{m-1} (1-\mu_{\phi,L})^m \quad (51)$$

Substituting G in $\mathbb{P}[\hat{W}_i = m]$ we get,

$$\begin{aligned} \mathbb{P}[\hat{W}_i = m] &= (1-p_a)^{m-1} \mu_{\phi,L} (1-\mu_{\phi,L})^{m-1} + \\ &\quad p_a (1-p_a)^{m-1} (1-\mu_{\phi,L})^m \\ &= q_s (1-q_s)^{m-1} \text{ for } m=1, 2, \dots \end{aligned} \quad (52)$$

where, $q_s = \mu_{\phi,L} + p_a (1-\mu_{\phi,L})$. We can obtain $\mathbb{E}[\hat{W}_i] = \sum_{m=1}^{\infty} m [q_s (1-q_s)^{m-1}]$. Replacing $1-q_s = t$, we get,

$$\mathbb{E}[\hat{W}_i] = \sum_{m=1}^{\infty} m [q_s (1-q_s)^{m-1}] = \frac{1}{1-t} = \frac{1}{q_s} \quad (53)$$

Similarly for V_i we can obtain $\mathbb{E}[V_i] = \sum_{n=0}^{\infty} n [p_a (1-p_a)^n]$. Replacing $1-p_a = w$, we get,

$$\mathbb{E}[V_i] = \sum_{n=0}^{\infty} n(1-w)w^n = \frac{w}{1-w} \approx Z_a, \quad (54)$$

We can obtain $\mathbb{E}[W_i] = \sum_{m=1}^{\infty} m \left[\mu_{\phi,L} (1 - \mu_{\phi,L})^{m-1} \right]$. Replacing $1 - \mu_{\phi,L} = v$, we get,

$$\mathbb{E}[W_i] = \sum_{m=1}^{\infty} m \left[\mu_{\phi,L} (1 - \mu_{\phi,L})^{m-1} \right] = \frac{1}{1-v} = \frac{1}{\mu_{\phi,L}} \quad (55)$$

Thus, the upper bound of PAoI measured at the typical IoT is given by $A_{i,P}^U = \mathbb{E}[A_i(\beta, E_{th}) : \phi]$. From (8) and (9), $A_{i,P}^U = \mathbb{E}[\hat{W}_{i-1}] + \mathbb{E}[V_i] + \mathbb{E}[W_i]$. From (53), (54) and (55), we get (21).

REFERENCES

- [1] S. Das and G. Ghatak, "A stochastic geometry analysis of energy-age tradeoff in wireless iot network," in *2024 22nd International Symposium on Modeling and Optimization in Mobile, Ad Hoc, and Wireless Networks (WiOpt)*, 2024, pp. 46–53.
- [2] R. D. Yates, Y. Sun, D. R. Brown, S. K. Kaul, E. Modiano, and S. Ulukus, "Age of information: An introduction and survey," *IEEE Journal on Selected Areas in Communications*, vol. 39, no. 5, pp. 1183–1210, 2021.
- [3] S. Kaul, R. Yates, and M. Gruteser, "Real-time status: How often should one update?" in *Proceedings IEEE INFOCOM*, 2012, pp. 2731–2735.
- [4] Y. Zhang and B. Ai, "Downlink transmission design for autonomous vehicles control using finite blocklength codes," in *2017 3rd IEEE International Conference on Computer and Communications (ICCC)*, 2017, pp. 753–757.
- [5] D. López-Pérez, M. Ding, H. Li, L. G. Giordano, G. Geraci, A. Garcia-Rodriguez, Z. Lin, and M. Hassan, "On the downlink performance of uav communications in dense cellular networks," in *2018 IEEE Global Communications Conference (GLOBECOM)*, 2018, pp. 1–7.
- [6] X. Lu, P. Wang, D. Niyato, D. I. Kim, and Z. Han, "Wireless networks with RF energy harvesting: A contemporary survey," *IEEE Communications Surveys and Tutorials*, vol. 17, no. 2, pp. 757–789, 2015.
- [7] R. Kumar, M. Gupta, K. Agrawal, and S. Prakriya, "NOMA based multiuser uplink signalling with energy harvesting IoT nodes," in *IEEE Region 10 Conference (TENCON)*, 2023, pp. 714–719.
- [8] M. A. Abd-Elmagid, N. Pappas, and H. S. Dhillon, "On the role of age of information in the internet of things," *IEEE Communications Magazine*, vol. 57, no. 12, pp. 72–77, 2019.
- [9] R. D. Yates and S. K. Kaul, "The age of information: Real-time status updating by multiple sources," *IEEE Transactions on Information Theory*, vol. 65, no. 3, pp. 1807–1827, 2019.
- [10] K. Chen, F. Benkhelifa, H. Gao, J. A. McCann, and J. Li, "Minimizing age of information in multihop energy-harvesting wireless sensor network," *IEEE Internet of Things Journal*, vol. 9, no. 24, pp. 25 736–25 751, 2022.
- [11] T. Zhu, J. Li, H. Gao, Y. Li, and Z. Cai, "AoI minimization data collection scheduling for battery-free wireless sensor networks," *IEEE Transactions on Mobile Computing*, vol. 22, no. 3, pp. 1343–1355, 2023.
- [12] G. Zhang, C. Shen, Q. Shi, B. Ai, and Z. Zhong, "AoI minimization for WSN data collection with periodic updating scheme," *IEEE Transactions on Wireless Communications*, vol. 22, no. 1, pp. 32–46, 2023.
- [13] S. Kim, R. Vyas, J. Bito, K. Niotaki, A. Collado, A. Georgiadis, and M. M. Tentzeris, "Ambient RF energy-harvesting technologies for self-sustainable standalone wireless sensor platforms," *Proceedings of the IEEE*, vol. 102, no. 11, pp. 1649–1666, 2014.
- [14] A. Hentati, W. Jaafar, J.-F. Frigon, and W. Ajib, "Analysis of the interdelivery time in IoT energy harvesting wireless sensor networks," *IEEE Internet of Things Journal*, vol. 8, no. 6, pp. 4920–4930, 2021.
- [15] A. Arafa, J. Yang, S. Ulukus, and H. V. Poor, "Age-minimal transmission for energy harvesting sensors with finite batteries: Online policies," *IEEE Transactions on Information Theory*, vol. 66, no. 1, pp. 534–556, 2020.
- [16] B. Yao, H. Gao, Y. Zhang, J. Wang, and J. Li, "Maximum AoI minimization for target monitoring in battery-free wireless sensor networks," *IEEE Transactions on Mobile Computing*, vol. 22, no. 8, pp. 4754–4772, 2023.
- [17] M. Costa, M. Codreanu, and A. Ephremides, "On the age of information in status update systems with packet management," *IEEE Transactions on Information Theory*, vol. 62, no. 4, pp. 1897–1910, 2016.
- [18] J. Wang, X. Cao, B. Yin, and Y. Cheng, "Sleep-wake sensor scheduling for minimizing AoI-penalty in industrial internet of things," *IEEE Internet of Things Journal*, vol. 9, no. 9, pp. 6404–6417, 2022.
- [19] X. Sun, F. Zhao, H. H. Yang, W. Zhan, X. Wang, and T. Q. S. Quek, "Optimizing age of information in random-access poisson networks," *IEEE Internet of Things Journal*, vol. 9, no. 9, pp. 6816–6829, 2022.
- [20] A. Sinha and R. Bhattacharjee, "Optimizing age-of-information in adversarial and stochastic environments," *IEEE Transactions on Information Theory*, vol. 68, no. 10, pp. 6860–6880, 2022.
- [21] N. Hirose, H. Iimori, K. Ishibashi, and G. T. F. D. Abreu, "Minimizing age of information in energy harvesting wireless sensor networks," *IEEE Access*, vol. 8, pp. 219 934–219 945, 2020.
- [22] P. D. Mankar, M. A. Abd-Elmagid, and H. S. Dhillon, "Spatial distribution of the mean peak age of information in wireless networks," *IEEE Transactions on Wireless Communications*, vol. 20, no. 7, pp. 4465–4479, 2021.
- [23] M. A. Abd-Elmagid, M. A. Kishk, and H. S. Dhillon, "Joint energy and SINR coverage in spatially clustered RF-powered IoT network," *IEEE Transactions on Green Communications and Networking*, vol. 3, no. 1, pp. 132–146, 2019.
- [24] H. H. Yang, A. Arafa, T. Q. S. Quek, and H. V. Poor, "Optimizing information freshness in wireless networks: A stochastic geometry approach," *IEEE Transactions on Mobile Computing*, vol. 20, no. 6, pp. 2269–2280, 2021.
- [25] —, "Spatiotemporal analysis for age of information in random access networks under last-come first-serve with replacement protocol," *IEEE Transactions on Wireless Communications*, vol. 21, no. 4, pp. 2813–2829, 2022.
- [26] O. M. Sleem, S. Leng, and A. Yener, "Age of information minimization in wireless powered stochastic energy harvesting networks," in *2020 54th Annual Conference on Information Sciences and Systems (CISS)*, 2020, pp. 1–6.
- [27] M. A. Abd-Elmagid and H. S. Dhillon, "Distributional properties of age of information in energy harvesting status update systems," in *2021 19th International Symposium on Modeling and Optimization in Mobile, Ad hoc, and Wireless Networks (WiOpt)*, 2021, pp. 1–8.